

UV missile plume signatures

Filip Neele*, Ric Schleijsen**

TNO Physics and Electronics Laboratory, The Hague, The Netherlands

ABSTRACT

As a result of the deployment of UV missile warning systems, recent years have seen an increasing interest in threat assessment in the UV band. Unfortunately, due to the different nature of the physical processes that are needed to describe a missile signature in the UV, available codes for the IR can not be applied. As a result, the development of a UV missile plume signature model was initiated.

This paper presents a model for the prediction of UV missile plume signatures, that takes into account relevant physical mechanisms in a missile plume. The model is based on first principles, predicting the radiance from CO-O chemiluminescence and hot particles in the plume, which are the dominant sources of radiation in the UV wavelength band considered. Scattering of radiation on particles in the plume can be important for particle-rich propellants and is accounted for in the code. The multiple scattering algorithm has been set up to handle any number of directions in an axi-symmetric medium; the algorithm presents a novel way of solving the radiative transfer problem.

Several examples are shown, to illustrate scattering processes in missile plumes. A number of validation tests are presented to show the model's performance. At this stage, comparisons with real data are under progress.

Keywords: UV, missile signatures, missile warning, radiative transfer

1. INTRODUCTION

The last decade has seen several operations that have demonstrated the ever-present threat of passively guided missiles for airborne platforms. In response to this threat, many nations have acquired (passive) missile warning sensors, most of which operate in the ultraviolet part of the spectrum. That part of the UV spectrum between about 250 and 290 nm (commonly referred to as the 'solar blind UV'), provides an excellent background for missile plume detection, as atmospheric ozone completely absorbs solar radiation. The absence of almost any background radiation allows good threat detection. However, due to the same atmospheric ozone, detection ranges are relatively short.

As a result of the deployment of UV missile warning systems, there is a need to assess or predict the system performance for each threat type. Models need to be developed that describe targets, atmosphere and sensor. Due to the particularities of both UV emission in the missile plume and propagation through the atmosphere, existing IR codes can not be used. To fill part of this gap in threat assessment capability, a model was developed that predicts the UV emission of missile plumes, operating in the solar blind UV band. When combined with models that account for atmospheric effects (transmission, scattering) and the sensor, the model can be used to predict detection of shoulder-fired anti-air missiles by UV missile warning sensors.

The model that is presented here takes into account chemiluminescence between CO and O, which is the dominant source of UV emission in the solar blind UV band, and scattering at particles in the plume. The latter can not be ignored, especially for near nose-on aspect angles. The radiative transfer in the plume is treated differently from current models, in both the treatment of direction dependence of the radiation field and the computation of consecutive orders of scattering. No interpolation schemes are used for the angular dependence of the radiation field in the plume.

* neele@fel.tno.nl; phone +31 70 374 0461; fax +31 70 374 0654

** schleijsen@fel.tno.nl; phone +31 70 374 0045; fax +31 70 374 0654

TNO Physics and electronics laboratory, P.O. Box 96864, 2509 JG Den Haag, The Netherlands

Section 2 describes the outline of the model and discusses the various physical processes that are relevant in the solar blind UV. The model is applied to several test cases. For the first test case the analytical solution of the radiative transfer is available (section 3), providing a test for the scattering algorithm. In section 4 test media are defined, to compare the results of the model presented here with those from a model that uses different solution schemes. These latter test media are representative of the conditions in missile plumes.

2. MODEL OUTLINE

The UV radiance model is a line model, as it computes the radiation emitted at a single wavelength in the range 250 – 290 nm. The (implicit) wavelength interval width is 1 nm. The wavelength limits are imposed by the limits in the data describing the CO-O chemiluminescence (see below) and by the possible onset near 300 nm of OH chemiluminescence for wavelengths, which is not included in the code. The model can be used to compute both the integrated plume intensity, as well as the spatial radiant intensity variation over the plume. Spectral variations can be predicted by running the code several times at different wavelengths.

The computation of the radiation field inside the plume is done in three steps. Once the plume structure and composition are known (these are to be supplied by flow field codes as REP^{1,2} or SOBOAT³, the code performs the following tasks:

1. Generation of the grid on which the plume is represented. Two grids are used, one spatial and one directional grid. These grids can be specified independently. The only restrictions on spatial size and number of directions accounted for in the radiation field are computer memory and computation time.
2. Computation of radiation from hot particles and chemiluminescence. These two sources of radiation can be computed using straightforward physics; the radiation field from these sources is isotropic. The contribution from the nozzle and the combustion chamber is included at this stage. This contribution is expressed as the radiation from a blackbody at a specified temperature. The contribution from the combustion chamber is represented by the blackbody radiation from the exit plane, which has a temperature known from the flow field calculations. The nozzle and combustion chamber can contribute to the total intensity of the plume, even for small off-nose aspect angles, as this radiation may be scattered in the plume, towards the observer.
3. Scattering in the plume. This is the most time-consuming task. Scattering must be taken into account, as particles in the plume cause a significant re-distribution of the radiation inside the plume. Missile plumes are most often observed at near-nose on aspect angles and it is at these aspect angles, that scattering in the plume is most important.

These tasks are detailed in the following sections.

2.1 SPATIAL AND DIRECTIONAL GRIDS

The UV emission code has been developed for axi-symmetric plumes. Therefore, the plume flow field (temperature, chemical composition, etc.) needs to be stored only on a single cross-section through the plume, parallel to the plume axis (see Figure 1). This is also true for the (anisotropic) radiation field: the intensity in any given direction, at any location inside the 3-D plume can be stored on the cross-section indicated in the figure. Even though the scattering calculations are performed in three dimensions, all references to the plume flow field and radiation field are related to their corresponding values on this cross-section. This set-up minimises computer memory usage.

To describe the directional dependence of the radiation field, the 4π steradians of solid angle at each grid point are discretised by dividing the unit sphere into N cells of (almost) equal area. There are no explicit restrictions on the number of directions N , apart from computational aspects (computer memory). The number of directions is not explicitly related to the spatial grid.

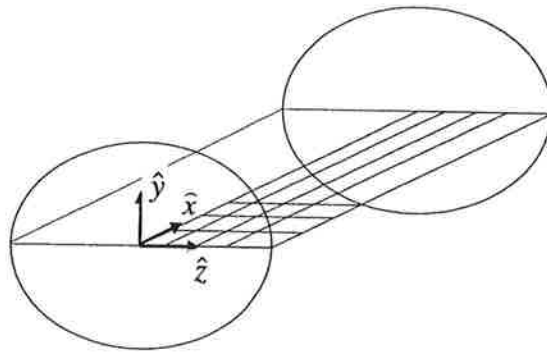


Figure 1. Schematic representation of the spatial grid used to store both the plume structure and composition, and the direction-dependent radiation field. The nozzle is at $x=0$, with the x axis pointing away from the nozzle.

2.2 CHEMILUMINESCENCE

CO-O chemiluminescence in the plume depends on the concentration of CO and O, and on temperature. Given the conditions at the nozzle exit plane, plume flow field codes, such a REP, provide the information necessary to compute the radiation emitted by the combination of CO and O. The relations given are empirical⁴. Figure 2 shows the temperature and wavelength dependence of the chemiluminescent intensity.

2.3 NOZZLE AND EXIT PLANE

Contributions from the nozzle and exit plane must be taken into account. If the nozzle is assumed to be at the temperature of the gases at the exit plane, radiant intensities are comparable with those in the plume. In addition, the radiation from the nozzle and exit plane can be scattered by the plume into directions that do not have a direct line of sight with the nozzle.

In the code, the nozzle and exit plane are represented by black bodies, with a temperature equal to that of the gases at the exit plane. The exit plane radiates only into the hemisphere pointed away from the nozzle, while the nozzle exterior radiates only away from the plume length axis. All nozzle surface are assumed to behave as Lambertian surfaces.

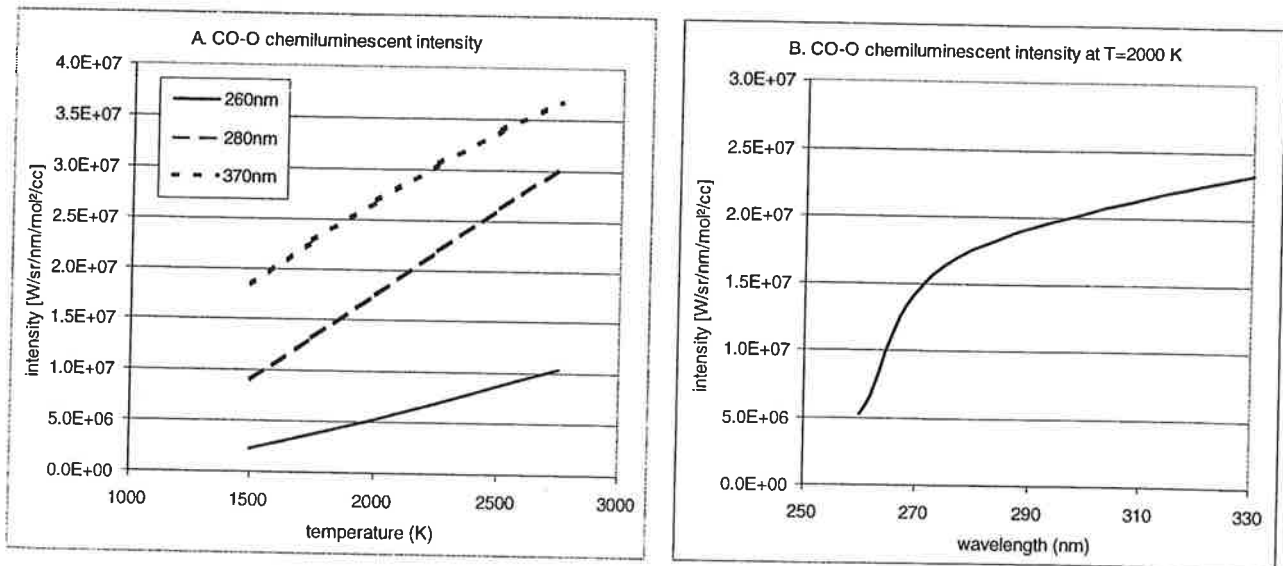


Figure 2. Intensity of the CO-O chemiluminescence as a function of temperature (a) and wavelength (b). The relations were obtained by experiment⁴.

2.4 PARTICLES

Particles in the plume play a central role in the radiative transfer in the plume. The particles are often aluminium oxide, resulting from aluminium added to the propellant to increase thrust.

All optical properties can be derived from the particle refractive index, using Mie scattering theory. For wavelengths below 300 nm and particle sizes in the range of 0.1 – 100 μm , this theory describes the scattering processes⁵. For a given particle size distribution, such as that exists in an exhaust plume, this theory can be used to compute the effective optical properties and scattering phase function. The only restriction in applying Mie theory is that particles are assumed to be spherical. However, since particle measurements inside exhaust plumes are difficult and data are not readily available, particle sphericity is a necessary assumption.

Figure 3 shows the wavelength dependence of the refractive index of alumina particles⁶; real and imaginary parts of the refractive index are shown separately. The data also show the temperature dependence of the refractive index. This dependence is significant for the temperature range in an exhaust plumes, where temperatures may increase to 2500 K. The data show that for temperature above about 2300 K there is a strong increase in both real and imaginary parts of the refractive index.

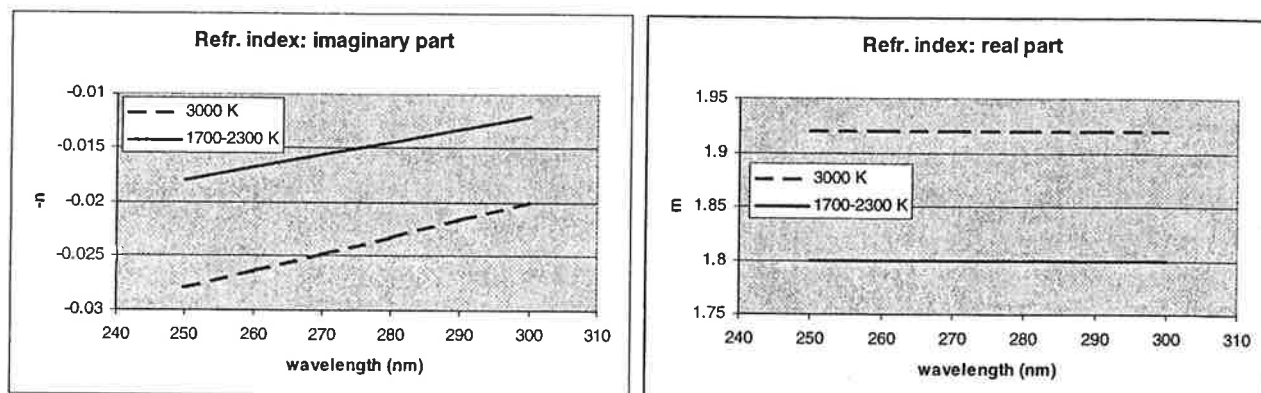


Figure 3. Real and imaginary parts of the refractive index of Al_2O_3 (ref. 6). The two panels also show the temperature dependence that is relevant to UV plume emission.

For a given particle size distribution, Mie theory is used to compute the scattering phase function. As an example, the Worster model⁷ is used to represent the size distribution. This model uses the following parameterisation for the size distribution in the plume

$$\frac{dN}{dD} = fAe^{-AD},$$

where the parameter f can be used to scale the total alumina content. The values $A = 1 \mu\text{m}$ and $f = 2.97 \cdot 10^6$ are used for the size distribution shown in Figure 4 and the scattering phase functions presented in Figure 5. Figure 4 shows the particle size distribution, by number, area and volume. For the parameter values given above, a particle density of $2.9 \cdot 10^6 / \text{cm}^3$, a total (projected) area of $4.7 \cdot 10^{-2} \text{ cm}^2/\text{cm}^3$ and a volume density of $9.3 \cdot 10^{-6} \text{ cm}^3/\text{cm}^3$ is found. This corresponds with a Al_2O_3 concentration of $2.17 \cdot 10^{17} \text{ molecules}/\text{cm}^3$, or $3.6 \cdot 10^{-7} \text{ mol}/\text{cm}^3$.

Figure 5 shows two scattering phase functions for this particle model, assuming aluminium oxide particles at a temperature of 2000 K and a wavelength of 280 nm. Particle albedo is 0.65, the extinction coefficient is 10.4 m^{-1} . This extinction value is almost the same as that, which would be found from a geometrical analysis, following from the total occluded area per unit area (4.7%). In this geometrical analysis, Babinet's principle⁸ must be invoked to account for the loss in both absorbed and refracted energy.

Figure 5 also shows the scattering phase function for the same particles, size distribution and wavelength, now at a temperature of 3000 K. The difference in refractive index results mainly in a lower albedo of 0.61 (giving rise to different emission and absorption characteristics); the scattering phase function is not significantly different from that at a lower temperature.

The scattering phase functions show that the scattering in the exhaust plume is predominantly forward, with a small backscattering peak. The latter phenomenon is important for near-nose-on missile signatures. Radiation from the hot

nozzle and combustion chamber is scattered in the outer layers of the plume, at large scattering angles, towards near nose-on aspects. The variation in the scattering phase functions for wavelengths between 250 and 300 nm is of the same order of magnitude as the variation present in Figure 5.

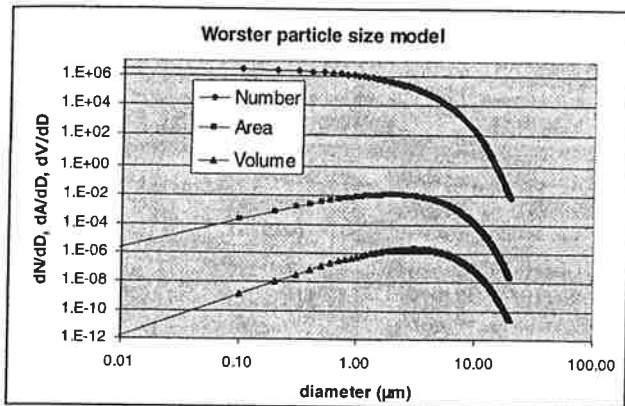


Figure 4. Worster particle size distribution model⁷, with $A = 1 \mu\text{m}$ and $f = 2.97 \cdot 10^6$ (see text). Curves show the distribution with respect to number, area and volume.

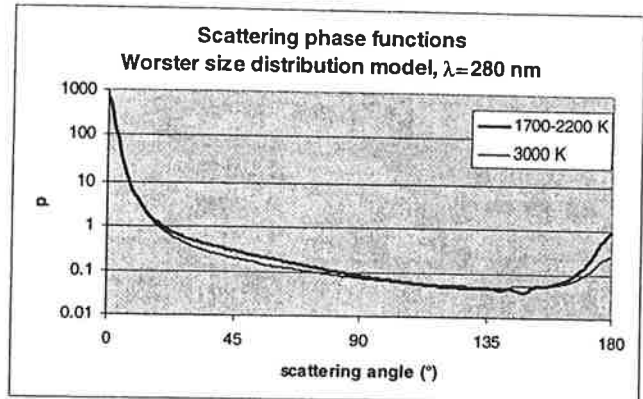


Figure 5. Scattering phase functions computed for $\lambda=280 \text{ nm}$, for two temperatures (i.e., different particle refractive indices). Note the strong forward scattering peak.

2.5 SCATTERING ALGORITHM

Once the contributions from the nozzle, exit plane, hot particles and chemiluminescence and the scattering properties of the particles have been computed, scattering in the plume must be treated. The scattering algorithm in the plume emission code differs from most of the currently used radiative transfer codes. The central problem in solving the radiative transfer is to obtain sufficient angular resolution. Two-flux or six-flux methods compute the radiance field in two or six directions, which is insufficient for the present problem, where a detailed description of near nose-on signature is required. To overcome computational load and memory problems, several methods have been proposed to increase the number of directions with, for example, quadrature schemes^{9,10} or spherical harmonics¹¹. The scattering algorithm used in the present model simply divides the total of 4π solid angle into N direction bins. At each spatial grid point in the plume, the radiation field in these N directions is computed. With this approach, the spurious structure that may be introduced in the interpolation schemes mentioned above is avoided, at the cost of the requirement for a denser angular sampling.

A second difference with existing codes is the computation of successive orders of scattered energy. Rather than considering interaction only between neighbouring cells, one iteration of the scattering algorithm includes the interaction between all possible pairs of cells in the 3-D medium. Thus, for each cell in the three-dimensional plume, the energy received from every other cell in the plume is computed, taking into account transmission losses along the connecting lines of sight. Particle albedo controls the percentage of the absorbed energy that is scattered. The scattering phase function is used to distribute the scattered energy over the 4π sr of solid angle of the receiving cell.

At this stage, the relation between the spatial and directional grids becomes apparent. For any given pair of source-receiver cells, the receiving cell may be 'hit' by more than one direction cell at the emitter. In that case, all emitting cells for which the receiver is within the field of view are taken into account. In addition, by taking into account all possible source-receiver cells, many direction bins at each cell will be 'hit'. The redistribution of the absorbed energy over the direction bins then results in a radiation field smoothly varying with direction.

One complete loop over all possible combinations of cells in the plume produces a radiation field that is scattered once. This scattered field is added to the existing radiation field. After the first iteration of the scattering algorithm, all single scattering is included. Subsequent iterations of the algorithm produce higher orders of scattering. The scattering iterations are continued until the sum of the intensities at all cells, in all directions has changed by less than a specified amount (e.g., one percent) after one additional scattering iteration.

2.6 PLUME IMAGE GENERATION

Once the radiation field inside the plume is computed, one additional step must be taken to obtain the radiation field emitted by the plume. Due to its set-up, the scattering algorithm does not compute the radiation field emitted by the plume. Instead, it computes the radiation field at every spatial grid point in the plume. The total radiation emitted by the plume in any direction must be found by integrating along the corresponding lines of sight (LOS) through the plume.

The image algorithm, for a given LOS (with the direction specified by the off-nose angle), integrates through the plume, generating an image of the plume as it is viewed by an observer. The algorithm can be viewed as propagating an image plane through the plume, in the direction of the LOS. The appropriate radiance values are accumulated along the way and transmission losses are accounted for. The integration commences on the far side of the plume (as seen from the observer) and is continued through the plume to the near side of the plume. Pixel size on the image plane is that of the spatial grid in the plume, with a correction due to the projection cosine.

In the integration over the LOS, the only factor that needs to be taken into account is the transmission loss of the radiance through the plume. Forward scattering coefficients are included implicitly, as that part of the radiative transfer has been accounted for in the scattering algorithm and are included in each radiance value in any given direction, at any position in the plume. Once the scattering algorithm is completed, all forward scattering contributions along any LOS are included in the radiance field in the plume.

3. TEST CASE: ISOTROPIC SCATTERING IN AN INFINITE SLAB

Van de Hulst¹² provides a test case for radiative transfer through an infinitely wide slab with homogeneously distributed sources and scatterers. The radiative transfer through this medium can be described analytically. The solution gives the angle-dependent intensity, as a function of the scattering albedo in the slab. Figure 6 shows the geometry of the problem. The slab has unit optical thickness.

The code developed for the axisymmetric plumes was adapted and applied to the van de Hulst geometry. The results are shown in Figure 7, along with the analytical solution. Curves of intensity versus aspect angle are shown for several values of the scattering albedo. The results are normalised with the intensity at $\mu = \cos(\theta) = 0$ for albedo zero (i.e., no scattering). The variation in the intensity with aspect angle is the result of a trade-off in the length of the optical path through the medium and the absorption and emission along that optical path. As a result, low intensities are observed for perpendicular look-down angles. The maximum in the curves arises from the phenomenon that the scattered radiation field decreases in magnitude towards the surface of the medium, due to the smaller number of sources¹².

The results in Figure 7 show that the scattering algorithm provides an accurate representation of the true scattering processes. Even for an albedo near unity, which is most demanding for any scattering algorithm, the code accurately reproduces the exact solution. The number of iterations required to reach this level of agreement varies with the albedo: for higher values of the albedo more iterations, i.e., higher orders of scattering (for the present model ten orders of scattering for an albedo of 1.0), are required to obtain an accurate representation of the solution.

4. PLUME TEST CASES

To further test the model, test media derived from a generic missile plume were used¹¹. Figure 8 shows the positions in the generic plume that were sampled to provide the data for the four media. The four media represent different regions of a missile plume: close to the nozzle (medium 1), between the nozzle and the afterburning zone (medium 2), the afterburning region (medium 3) and the relatively cold parts down the plume axis (medium 4). The structure in the generic plume along each of the four cross-sections was used to generate a cylindrical, 1-D, medium. The extinction, temperature and chemiluminescence in the four test media is shown in Figure 9. The scattering in these media is characterised by an albedo of 0.8 and a scattering phase function given by a Henyey-Greenstein function with asymmetry parameter g of 0.8. The level of scattering is linearly related to the extinction coefficient. The media dimensions were 0.8 m in length and 0.06 m in radius. The spatial grid size was 0.015 m, while the direction bins had a diameter of about 8° (resulting in a total of 616 direction bins at each spatial grid point).

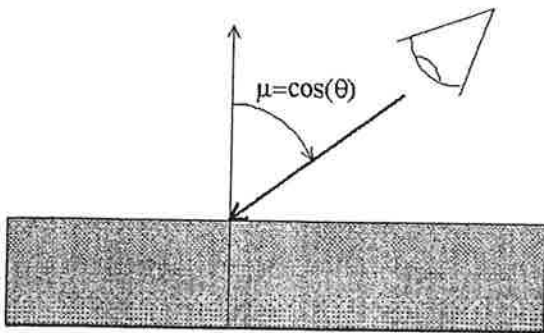


Figure 6. Geometry of the test case, given by van de Hulst¹². The scattering medium is an infinite slab, with embedded (homogeneously distributed) sources and scatterers. The intensity is computed as a function of aspect angle $\mu = \cos(\theta)$.

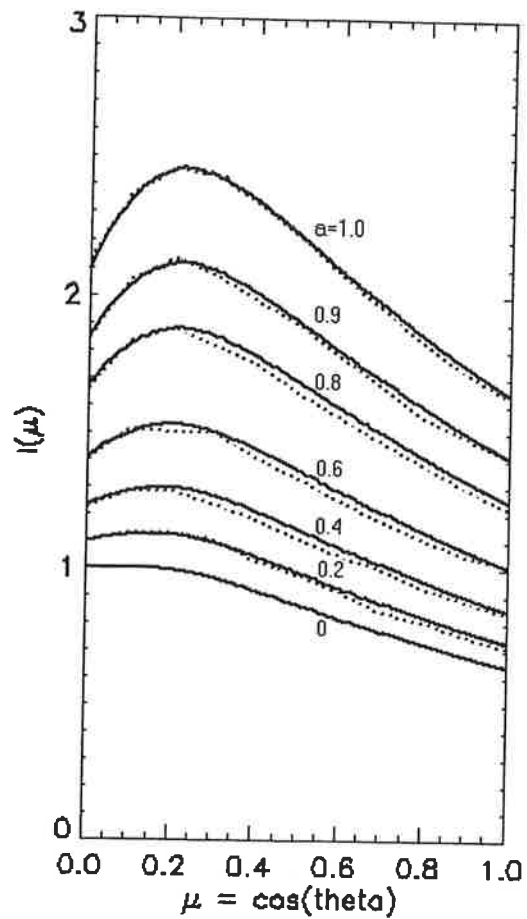


Figure 7. (Right) Intensity as a function of aspect angle ($\mu = \cos(\theta)$), for the van de Hulst test case, for different values of the scattering albedo. Dashed curves represent the exact solution. All curves have been normalised with respect to the intensity at $\mu = 0$ for a scattering albedo of zero.

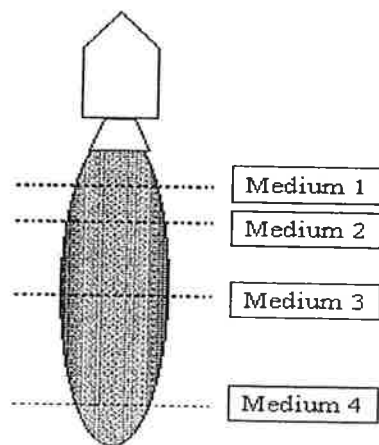


Figure 8. A generic missile plume was used to generate four test media: at each of the positions indicated the structure and composition in the generic plume were used to create a cylindrical plume.

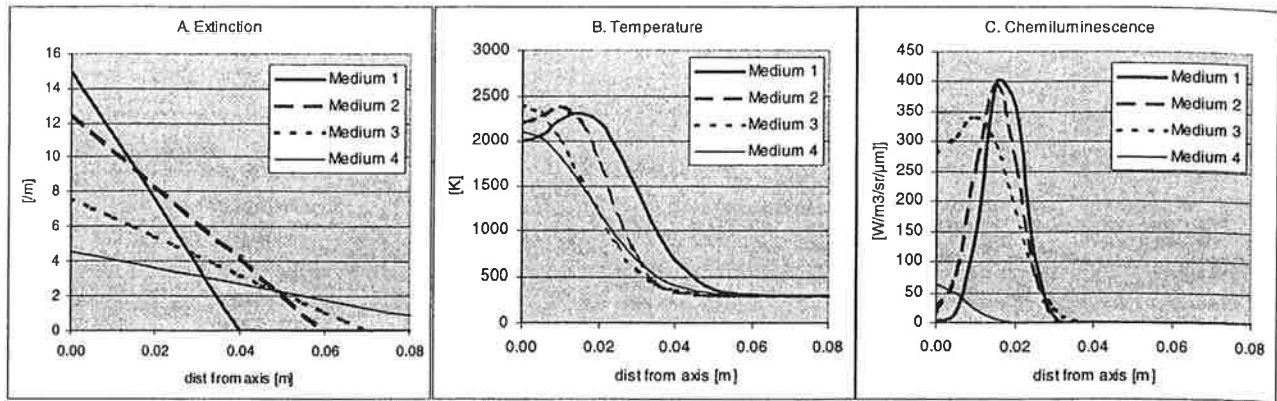


Figure 9. Extinction (a), temperature (b) and chemiluminescence (c) as a function of distance from the medium axis for each of the four test media. See also ref. 11.

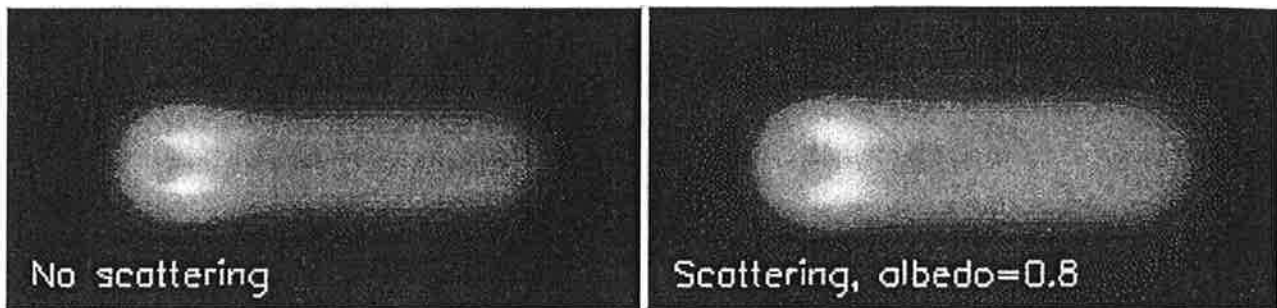


Figure 10. Cross-sections through medium 2 at an off-nose angle of 10° . The bright annular region corresponds to the region of high temperatures at about 2 cm from the medium axis (see Figure 9). The left panel shows the medium for an albedo of zero (no scattering); the right panel shows the medium with albedo 0.8 (strong scattering). The length of the medium is 0.8 m.

The aim of the four test media was to compare the result from the present code with that from a code developed at ONERA¹¹, that employs a different scheme to solve the radiative transfer. The plume UV emission code presented in this paper was used to predict the total intensity from the test plumes as a function of aspect angle, as well as to predict the variation of plume radiant intensity across the 1-D cylindrical medium.

Figure 10 shows an image generated for medium 2, for an albedo of zero, implying no scattering, and for an albedo of 0.8 (strong scattering). The difference between the two images shows that scattering causes the plume to become wider, as well as more intense. Although part of the higher intensity originates from radiation from hot particles (which is zero when the albedo is zero), the scattering also redirects energy towards the observer, resulting in a more intense and wider plume.

4.1 CROSS SECTIONS

Figure 11 shows cross sections through images as shown in Figure 10, for aspect angles of 20° and 90° . The length of the test media (0.8 m) was chosen such, that the radiation field halfway the medium was unperturbed by the fact that the medium has finite length. The cross sections shown below were taken at an unperturbed position. Two curves are shown in Figure 11 for each aspect angle, representing the results from the model presented here and the ONERA model¹¹. Scattering albedo was 0.8, representative of strong scattering. Four iterations were required to reach convergence. There is good agreement between the two emission models. Similar results, for medium 3, are shown in Figure 12. This figure can be compared directly to figure 9 of ref. 11.

The significance of scattering is illustrated clearly in Figure 13, which shows the aspect-angle dependence of the total intensity of test medium 4. The different curves show the total intensity for different orders of scattering included. For this medium, convergence of the scattering calculations was achieved after two iterations; including third and higher

orders of scattering produced no significant change in the radiation field. The figure shows that scattering, for this medium, accounts for about 10% of the total intensity.

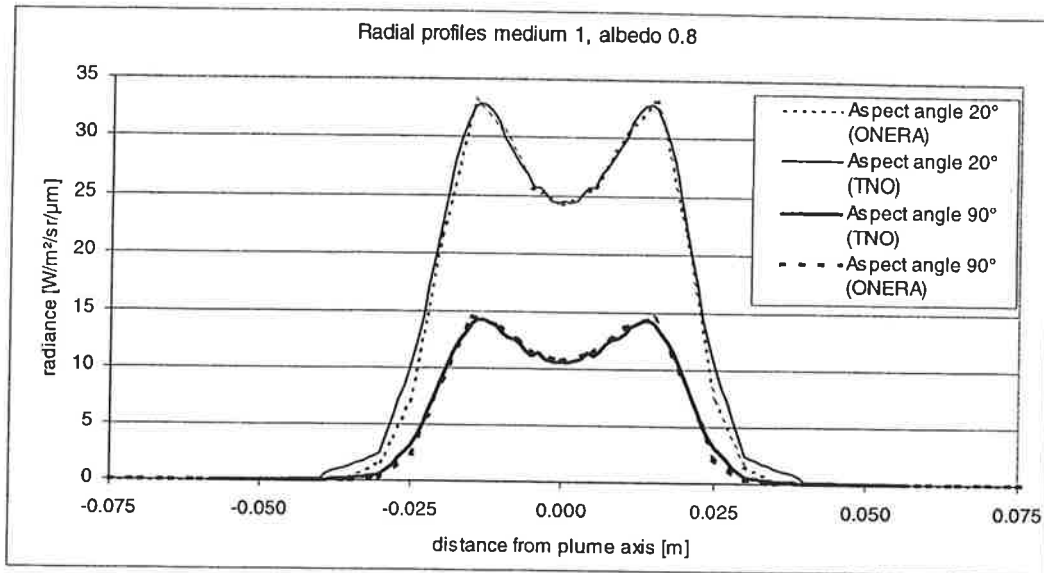


Figure 11. Cross-sections of the radiant intensity of medium 1, at off-nose angles of 20° and 90°. The results from the model presented here, as well as those from the ONERA UV emission model are shown. The predictions from the two models agree closely.

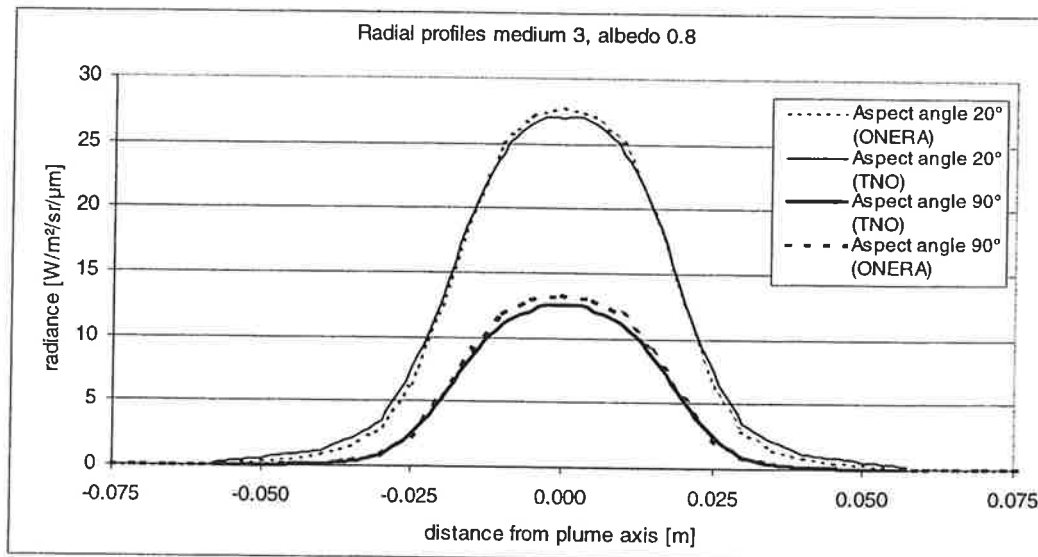


Figure 12. As Figure 11, now for medium 3, which represents the afterburning region in a missile plume.

4.2 MASKING EFFECTS

As stated above, in the UV wavelength band it is essential to accurately represent the scattering inside the plume. Scattering in the outer parts of the plume (relatively cold, and significantly less intense than the hot plume core) results in a much higher than expected visibility of the plume at near nose-on wavelengths. At these aspect angles the missile body hides the hot and intense core from direct view, resulting in almost zero direct radiation reaching the observer. The scattering in the outer parts of the plume counters this effect.

The results in Figure 14 illustrate this. Shown is the total intensity of the plume, as a function of the radius of a mask, that is positioned over the centre of the plume image. As the mask radius is increased, a larger portion of the hot core is

removed from direct view. For mask radii larger than about 4 cm only energy scattered in the plume reaches the observer (see the profiles of temperature and chemiluminescence in Figure 9). Two sets of curves are shown in Figure 14, representing a plume without particles ('no scattering') and a plume with strong scattering ('albedo 0.8'). For each case, the results from the model presented here are shown, along with those from the ONERA model¹¹. The two sets of curves represent two scattering extremes and show that, at least for particle-rich exhaust gases, scattering may not be ignored when assessing the UV signature of a missile.

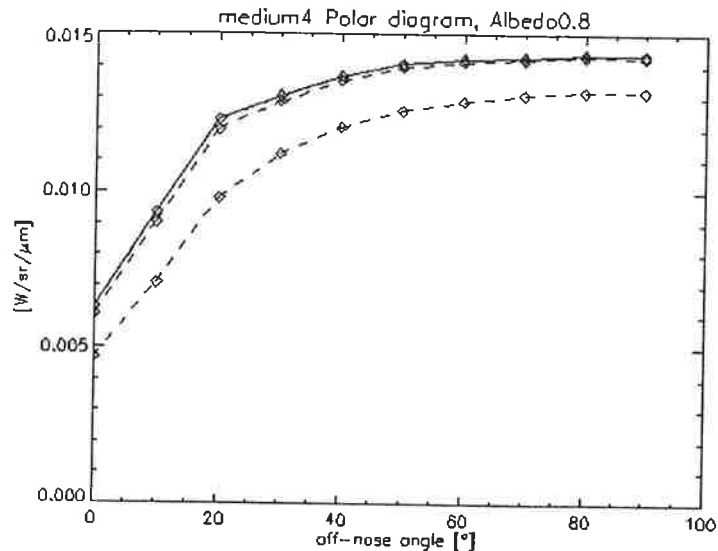


Figure 13. Polar diagram for medium 4. The curves represent different orders of scattering taken into account: no scattering (bottom curve), single scattering (middle curve), energy scattered twice (solid curve). Including third and higher scattering orders does not change the result.

5. DISCUSSION

This paper presents a new model for the computation of the emission of missile plumes at ultraviolet wavelengths, in the band between 250 and 300 nm. The model has been developed to assess the visibility of missiles for missile warning sensors operating in the UV band.

The model is based on a combination of first principles and experimental data. At the wavelengths involved, scattering in the plume is strong and can not be ignored. The scattering algorithm in the program can handle any number of directions, to solve the radiative transfer in the plume to a desired level of accuracy.

The model has been tested against several test cases. The first, an isotropic scattering problem for which the analytical solution is known, shows that the model accurately describes the scattering processes in the plume. The second test case consists of a series of cylindrical media, representative of different parts of a generic missile plume. Results from the present model were compared with those from a model that is based on different algorithms for solving the radiative transfer. The results from the two models agree closely. The latter test case does not provide a rigorous validation of the model. A true model validation would include a comparison with observed plume signatures. However, these data are often subject to restrictions or difficult to obtain. The test cases shown here are as close as possible to a true validation, without observed data.

Current work on this model are aimed at continued validation, using both test cases from the literature and further comparisons with other UV emission models. A true model validation, comparison of model predictions with measured plume signatures, will be performed.

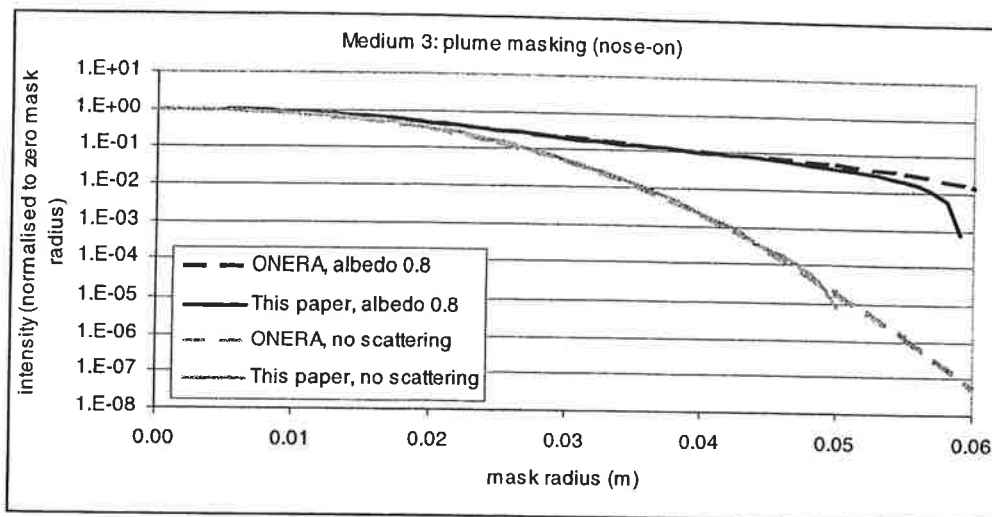


Figure 14. Total radiance for nose-on aspect view, as a function of the radius of a mask (missile body). Curves are shown for plumes with ('albedo 0.8') and without particles ('no scattering'). The results show that for near nose-on views scattering in the outer parts of the plume can significantly increase the plume signature. The results from the model presented here and that of ONERA are in good agreement. It should be noted that the results have been normalised with respect to the intensity for zero mask radius. Note that the vertical axis has a logarithmic scale.

ACKNOWLEDGEMENTS

The authors are grateful to Dr A. Roblin of ONERA, France, for stimulating discussions, his co-operation in defining the test cases and providing results from the ONERA code. The work described here has been done under contracts from the Royal Netherlands Air Force.

REFERENCES

1. J.M. Cousins, Calculation of conditions in an axi-symmetric rocket exhaust plume: the REP3 computer program, DERA technical report 218, Westcott, United Kingdom, 1982.
2. D.A.B. Fuggie, D.P. Hills, A. Christopher and H. Mace, An efficient procedure for solving the chemical species transport equations in the computer program REP3, DERA technical report 262, Westcott, United Kingdom, 1983.
3. M. Selzer, SoBOAT: a Numerical Code for the Prediction of Gas-particle flow in the vicinity of Nozzle Boattails of Rocket Motors, IABG report, Wehrtechnische Analysen (WA), Abteilung WA 45, B-WA 4506/01, 2000.
4. M. Slack and A. Grillo, High temperature rate coefficient measurements of CO+O chemiluminescence, *Comb. Flame*, 59, 189-196, 1985.
5. E.J. McCartney, *Optics of the atmosphere*, Wiley, New York, 1976.
6. A.J. Saladino and R.C. Farmer, Radiation/convection coupling in rocket motor and plume analysis, SECA report SECA-FR-93-10, Huntsville, 1993.
7. R.B. Lyons, J. Wormhoudt and C.E. Kolb, Calculation of visible radiation from missile plumes, AIAA paper 81-1111, 1981.
8. H.C. van de Hulst, *Multiple light scattering*, Academic Press, New York, 1983.
9. C.E. Siewert, "A concise and accurate solution to Chandrasekhar's basic problem in radiative transfer", *J.Q.R.S.R.T.*, 64, 109-130, 2000.
10. F.M. Schulz and K. Stamnes, "Angular distribution of the Stokes vector in a plane-parallel, vertically inhomogeneous medium in the vector discrete ordinate radiative transfer (VDISORT) model", *J.Q.R.S.R.T.*, 65, 609-620, 2000.
11. P.-E. Baudoux, A. Roblin and P. Chervet, "New approach for radiative-transfer computations in axisymmetric scattering hot media", *J. Thermophys. Heat Transfer*, 15, 317-325, 2001.
12. H.C. van de Hulst, *Light scattering by small particles*, Wiley, New York, 1957.



PROCEEDINGS OF SPIE
SPIE—The International Society for Optical Engineering

Targets and Backgrounds VIII: Characterization and Representation

Wendell R. Watkins
Dieter Clement
William R. Reynolds
Chairs/Editors

1–3 April 2002
Orlando, USA

Sponsored and Published by
SPIE—The International Society for Optical Engineering



Volume 4718

SPIE is an international technical society dedicated to advancing engineering and scientific applications of optical, photonic, imaging, electronic, and optoelectronic technologies.